Determination of Parameters in the Universal Induction Motor Model

Article *in* IEEE Transactions on Industry Applications · March 2009

DOI: 10.1109/TIA.2008.2009481 · Source: IEEE Xplore

CITATIONS
113

READS
1,762

3 authors:

Behrooz Mirafzal
Kansas State University
154 PUBLICATIONS **4,397** CITATIONS
SEE PROFILE

Gary leonard Skibinski
Rockwell Automation
92 PUBLICATIONS **5,861** CITATIONS
SEE PROFILE

Rangarajan Tallam
Rockwell Automation
62 PUBLICATIONS **2,926** CITATIONS
SEE PROFILE

Determination of Parameters in the Universal Induction Motor Model

Behrooz Mirafzal, *Senior Member, IEEE*, Gary L. Skibinski, and Rangarajan M. Tallam, *Senior Member, IEEE*

***Abstract*—A systematic procedure to determine the parameters of a previously proposed low- to high-frequency induction motor model is presented. An analysis of the high-frequency behavior with regard to the impact of magnetic core selection, parasitic interturn and winding-to-frame capacitors, and skin effects of windings is investigated in greater detail for the proposed universal model of an induction motor. The model is universal in the sense that it is derived by extending the low-frequency standard T-equivalent circuit (IEEE Standard 112) to include high-frequency effects under both common- and differential-mode domains and can be used for transient reflected-wave studies and electromagnetic interference emissions in motor drive systems. A test-based method and an analytical approach, which are useful in application and design stages, respectively, are presented to determine the frequency characteristics of the induction motor. Findings of the investigation were verified experimentally with results presented in this paper.**

***Index Terms*—Electromagnetic interference (EMI), high-frequency model, induction motor, reflected wave, transient overvoltage.**

I. Introduction

In AC motor-drive systems, which generally consist of an ac–ac converter, a cable, and an ac electric motor, fast semiconductor devices (e.g., insulated-gate bipolar transistors) are desirable in order to reduce switching losses and consequently obtain higher efficiency in a compact package. Fast switching means shorter voltage rise time, which can lead to the reflected-wave phenomenon as well as high-frequency leakage currents through the system's stray capacitors [1]–[7]. Reflected waves cause voltage spikes at the motor terminals, and the high-frequency leakage currents cause electromagnetic interference (EMI). These two phenomena are commonly modeled as two decoupled single-line circuits, namely, differential mode (DM) and common mode (CM); however, the secondary (consequent) phenomena may be overlooked in this type of analysis. Moreover, three-phase pulsewidth modulators (PWMs) can interact with cable and motor models, creating up to three times the bus voltage at the motor terminals, depending on the dwell-time spacing between line-to-line voltage pulses [8]. Dwell time must be estimated offline before a single-line model can be used. Thus, it is advantageous to simulate a three-phase modulator that directly interacts with three-phase cable and motor circuits for any inverter operating point. Various three-phase control algorithms such as PWM sine triangle, sine triangle with third harmonic, space vector, and two-phase modulation can then be studied for instantaneous line-to-line and line-to-ground waveform simulation. Lastly, the use of active front-end converters, with its switching action unsynchronized with the inverter, make single-line models less accurate for determining line-to-line and line-to-ground voltage stress on long cables [9]. Thus, a three-phase system model has advantages versus a single-line model in many ac motor-drive studies.

There are many investigations on modeling induction motors at high frequencies such as [1]–[8]. The existing problem in the field today is that researchers are proposing various individual high-frequency circuits to describe reflected wave, CM current, bearing current, and shaft voltage. Many of these circuits only address one issue and, in addition, ignore the low-frequency desired electrical stator quantities and rotor mechanical output quantities. In [2], the authors have proposed a high-frequency motor model that is built around the low-frequency d–q model. A close examination of the impedance response plots does not show a very good match between simulation and experimental results over a wide frequency range. A similar high-frequency motor model is also proposed in [5] and [6], albeit with better correlation between simulation and experiment. In the model proposed in [7], the motor slip cannot be varied; hence, its application to three-phase system simulations would be limited as it is desirable to observe transients and low-frequency effects in a single waveform. In an ac motor drive, as the load is varied, the PWM pulse pattern is adjusted to regulate the voltage, and this has an effect on reflected-wave and CM transients. Moreover, the useful frequency range of these models [2], [5]–[7] is limited to below the motor's antiresonance frequency. The model proposed in this paper includes the effect of antiresonance, which is important for high-frequency EMI studies and reflected-wave transients in ac motor-drive systems with short cables.

Fig. 1 shows the concept of building a universal model for induction motors based on the standard T-equivalent circuit (IEEE Standard 112) that was introduced in a previous investigation [4]. One significant objective in constructing this

Paper IPCSD-08-037, presented at the 2007 Industry Applications Society Annual Meeting, New Orleans, LA, September 23–27, and approved for publication in the IEEE Transactions on Industry Applications by the Electric Machines Committee of the IEEE Industry Applications Society. Manuscript submitted for review August 1, 2007 and released for publication April 18, 2008. Current version published January 21, 2009.

B. Mirafzal was with Allen-Bradley Drives Division, Rockwell Automation, Mequon, WI 53092 USA. He is now with the Department of Electrical and Computer Engineering, Florida International University, Miami, FL 33174 USA (e-mail: behrooz.mirafzal@fiu.edu).

G. L. Skibinski and R. M. Tallam are with Allen-Bradley Drives Division, Rockwell Automation, Mequon, WI 53092 USA (e-mail: glskibinski@ra.rockwell.com; rmtallam@ra.rockwell.com).

Color versions of one or more of the figures in this paper are available online at http://ieeexplore.ieee.org.

Digital Object Identifier 10.1109/TIA.2008.2009481

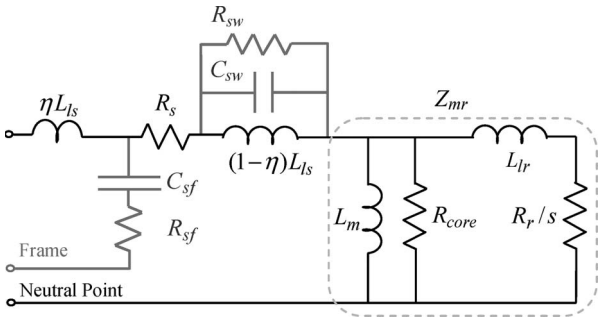

Fig. 1. Proposed universal model of induction motor per phase.

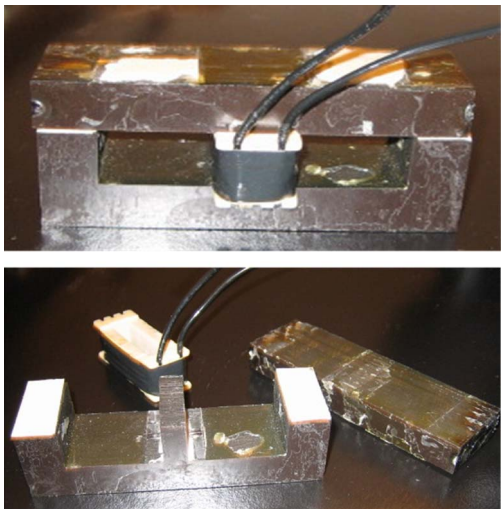

Fig. 2. Physical inductor, 800 turns of AWG 30, for two different cases: *Case (a)* with magnetic core and *Case (b)* without magnetic core.

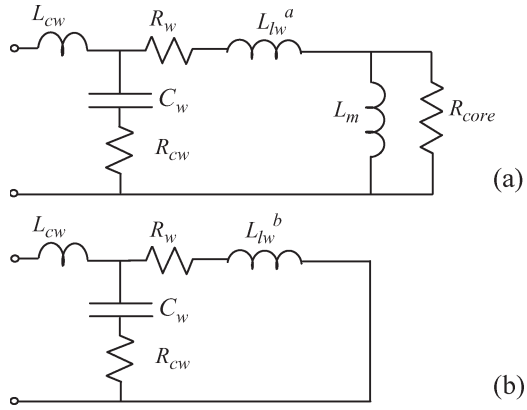

Fig. 3. Simple inductor equivalent circuits for two different cases: *Case (a)* with magnetic core and *Case (b)* without magnetic core.

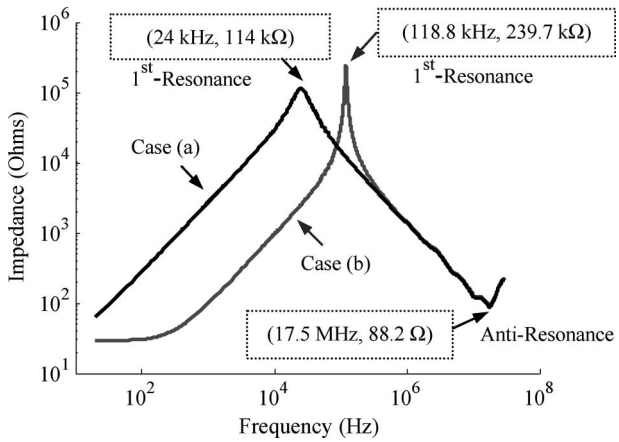

Fig. 4. Measured inductor impedance values versus frequency for two different cases: *Case (a)* with magnetic core and *Case (b)* without magnetic core.

accurate low- to high-frequency-range transfer function model of an induction motor was to build the needed mid- to high-frequency circuit model extension around the existing and accurate physical realizable quantities of the standard low-frequency equivalent circuit. Low-frequency T-equivalent circuit model parameters can be calculated from rotor-locked and no-load tests or in a design stage from mathematical calculations and finite element analysis [9], [10]. The main objective of this paper is to provide a systematic approach for obtaining the high-frequency components, which make it universal in a sense that it represents the motor's frequency response up to 10 MHz for both the CM and DM applications. *It should be noted that this model represents the motor behavior while powered by a PWM-based drive at a steady state condition or at a constant speed.*

In addition to this section, this paper contains five sections. In Section II, the impact of magnetic cores, parasitic interturn and winding-to-frame capacitors, and the skin and proximity effects of windings are studied using a simple electromagnetic circuit of an inductor. In Section III, the impact of Δ- and Y-connections on the effective winding-to-frame parasitic capacitors is investigated on a 100-hp induction motor. In Section IV, the findings of Section III are used to show how the parameters of the universal model of induction motors are determined using the motor frequency response.

II. Frequency Characteristics of Basic Electromagnetic Circuit

The frequency response of a simple inductor, shown in Fig. 2, is investigated in this section. This simple electromagnetic circuit can be used as the basis for the modeling and analysis of any electric machine. Moreover, the rotor circuit of electric machines does not have any contribution at high frequencies since no flux penetrates the rotor magnetic circuit [3]. Accordingly, a model developed for a simple inductor can be applied for the modeling and analysis of more complicated electromagnetic devices such as induction machines.

In Fig. 3, the proposed equivalent circuits of the winding shown in Fig. 2 are presented. The two equivalent circuits represent two cases, namely, *Case (a)*, winding with magnetic core, and *Case (b)*, winding without magnetic core. In Figs. 4 and 5, the impedance magnitudes and phase angles are shown for the aforementioned case studies. As can be observed, both the magnitudes and phases of the winding impedance at high frequencies are the same. Accordingly, it can be concluded that the winding impedance at high frequencies would be independent of the magnetic core materials. It should be noted that, in this particular magnetic device, the thickness of the bobbin is large such that the winding-to-frame capacitance value becomes much smaller than the interturn capacitance value. The

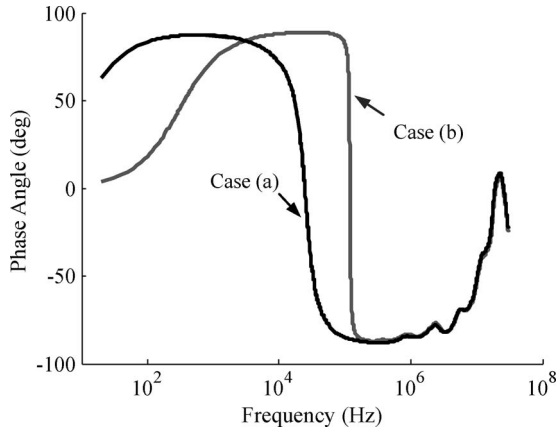

Fig. 5. Measured inductor impedance phase angles versus frequency for two different cases: *Case (a)* with magnetic core and *Case (b)* without magnetic core.

second observation is that the resonance bandwidth in *Case (a)* is wider than the corresponding bandwidth in *Case (b)* which is the inherent impact of the magnetic core losses.

As can be seen, the proposed equivalent circuit is built around the conventional magnetic equivalent circuit which is valid for low frequencies. The additional elements to the conventional circuit are winding stray capacitance C_w, antiresonance resistance $R_{\rm cw}$, and antiresonance leakage inductance $L_{\rm cw}$. The winding resistance value R_s as well as the magnetizing inductance L_m, leakage inductance $L_{\rm lw}$, and core-loss equivalent resistance $R_{\rm core}$ can be calculated from simple tests at the rated current and frequency. Notice that the magnetizing inductance, core-loss equivalent resistance, and winding resistance can be also analytically calculated from design specifications [6]. It should be noted that the skin effect below the first resonance frequency is somewhat significant. However, the skin effect on the winding's resistance at high frequencies is very significant and should be taken into account. Therefore, it is included as $R_{\rm cw}$ in this model. Winding parasitic capacitance C_w, can be obtained directly from knowing the resonance frequency and the magnetizing inductance. In the design stage, this capacitance value can best be estimated from finite element analysis. Then, the antiresonance leakage inductance $L_{\rm cw}$ and antiresonance resistance $R_{\rm cw}$ are obtained from knowing the frequency and impedance value of the second resonance, the so-called antiresonance frequency f_a point.

For the inductor shown in Fig. 2, the coil has 800 turns and a 29-Ω dc resistance, and the core has two parallel air gaps with (0.062 in) 1.575-mm heights and (0.75 in^2) 484-mm^2 cross sections. Using this information, the low-frequency components can be calculated for *Case (a)*. However, the LCR measurements can also be used to obtain the values of the low-frequency as well as high-frequency components. It should be noted that the winding-to-frame stray capacitance is negligible due to the existence of a relatively thick bobbin in this case study. Accordingly, C_w represents merely the interturn stray capacitance. This leads to the following procedure to obtain all circuit parameters shown in Fig. 3 from the impedance measurements shown in Figs. 4 and 5. These steps will be slightly different for electromagnetic devices in which the winding-to-frame stray capacitance is not negligible, which will be presented in Section IV.

TABLE I
INDUCTOR MODEL PARAMETER DETERMINATION, *CASE (a)* WITH THE MAGNETIC CORE

$\varphi_{\max} = 87.5^\circ$, $f = 580$ Hz, $\lvert Z\rvert = 1586\ \Omega$
$\varphi = 0^\circ \rightarrow f_r = 24$ kHz, $\lvert Z\rvert_{\max} = 114$ kΩ
$f_a = 17.5$ MHz, $\lvert Z\rvert_{\text{anti-r}} = 88.2\ \Omega$
$R_w = 29\ \Omega$
$L_{lw} + L_m = \sqrt{(\lvert Z\rvert^2 - R_w^2)/(2\pi f)} \rightarrow L_{lw} + L_m = 435$ mH
$C_w = 1/(L_{lw} + L_m)(2\pi f_r)^2 \rightarrow C_w = 101.1$ pF
$R_{cw} = \lvert Z\rvert_{\text{anti-r}} \rightarrow R_{cw} = 88.2\ \Omega$
$L_{cw} = 1/C_w(2\pi f_a)^2 \rightarrow L_{cw} = 0.76$ μH
$BW \neq 0 \rightarrow R_{core} = \lvert Z\rvert_{\max} \rightarrow R_{core} = 114$ kΩ

TABLE II
INDUCTOR MODEL PARAMETER DETERMINATION, *CASE (b)* WITHOUT THE MAGNETIC CORE

$\varphi_{\max} = 88.93^\circ$, $f = 27$ kHz, $\lvert Z\rvert = 2764\ \Omega$
$\varphi = 0^\circ \rightarrow f_r = 118.8$ kHz, $\lvert Z\rvert_{\max} = 239.7$ kΩ
$f_a = 17.5$ MHz, $\lvert Z\rvert_{\text{anti-r}} = 88.2\ \Omega$
$R_w = 29\ \Omega$
$L_{lw} = \sqrt{(\lvert Z\rvert^2 - R_w^2)/(2\pi f)} \rightarrow L_{lw} = 16.3$ mH
$C_w = 1/(L_{lw})(2\pi f_r)^2 \rightarrow C_w = 110.2$ pF
$R_{cw} = \lvert Z\rvert_{\text{anti-r}} \rightarrow R_{cw} = 88.2\ \Omega$
$L_{cw} = 1/C_w(2\pi f_a)^2 \rightarrow L_{cw} = 0.751$ μH

1) Obtain the frequency and corresponding impedance magnitude in which the impedance phase angle has its maximum value.
2) Obtain the frequency and impedance magnitude at the first resonance point.
3) Obtain the frequency and impedance magnitude at the antiresonance f_a point.

It should be emphasized that the accuracy in estimating the first resonance frequency f_r is very important in calculating the capacitance value of C_w. In order to reduce the estimation error of the first resonance frequency, both the amplitude $|Z|_{\max}$ and phase angle $\varphi = 0^\circ$ of impedance have to be taken into account. Because of the wide bandwidth in the first resonance in *Case (a)*, the chance of having an error in capturing the correct resonance frequency will be much higher than in *Case (b)*. Parameter determination data are given for *Cases (a)* and *(b)* in Tables I and II, respectively. Figs. 6 and 7 show that the modeled versus measured results are in good agreement.

A similar procedure can be applied for induction motors in order to calculate the high-frequency elements. However, in the case of induction motors, the parasitic winding-to-frame capacitance value is the dominant stray capacitance. This difference will be elaborated in the next section.

III. FREQUENCY CHARACTERISTICS OF INDUCTION MOTORS

In the low frequency range, the motor model at steady state conditions is best described by the T-equivalent circuit. It has been shown that the so-called universal model, which is

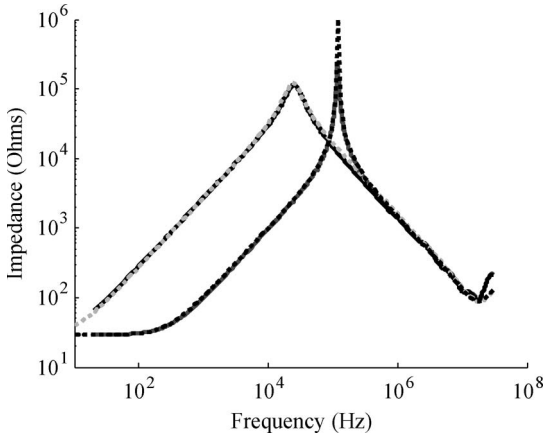

Fig. 6. (Dotted line) Modeled and (solid line) measured inductor impedance values versus frequency for two different cases: *Case (a)* with magnetic core and *Case (b)* without magnetic core.

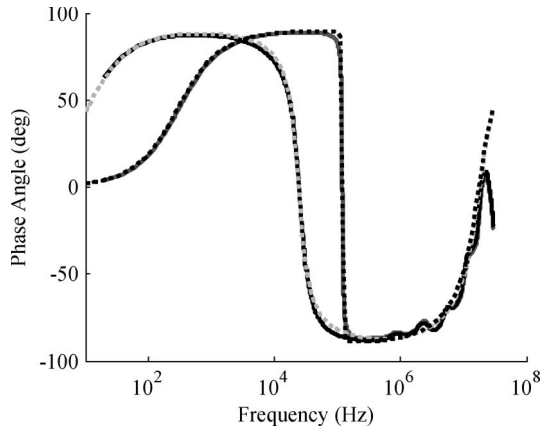

Fig. 7. (Dotted line) Modeled and (solid line) measured inductor impedance phase angles versus frequency for two different cases: *Case (a)* with magnetic core and *Case (b)* without magnetic core.

Fig. 8. Measured test setup of 100-hp inductor motor.

built around the T-equivalent circuit, is valid for up to several megahertz [4]. In this universal model, shown in Fig. 1, five elements are added. The challenge is how these new components can be determined. In this section, the high-frequency behavior of induction motors is studied by testing a 100-hp induction motor shown in Fig. 8. In this motor, all six leads of the stator windings were available. This makes it possible to

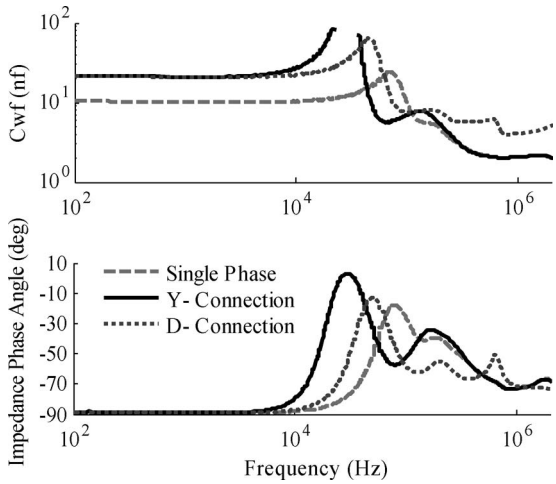

Fig. 9. Measured terminal to frame capacitance values in *nanofarads* and their corresponding impedance phase angles in degrees of the 100-hp motor.

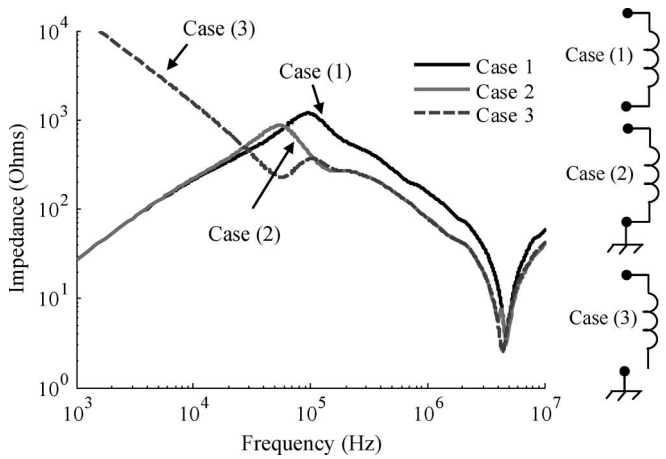

Fig. 10. Measured terminal impedance of single-phase winding of the 100-hp motor versus frequency.

investigate and study the impact of a single phase, as well as Δ- and Y-connections on the effective winding-to-frame parasitic capacitors $C_{\rm sf}$.

In Fig. 9, the measured winding-to-frame capacitance values versus frequency are shown for three different cases, single phase, Y-connection, and Δ-connection. These values were measured at the motor terminal with respect to the motor's frame. As can be observed, the winding-to-frame capacitance values for both Y- and Δ-connections are the same for frequencies below 10 kHz. However, at frequencies around 1 MHz, the capacitance value of the Y-connection becomes equal to the single-phase measured impedance. Notice that the capacitance value in the case of Δ-connection is twice the value of the other two cases at high frequencies. It should be noted that, in the mid frequency range, the measured capacitance value is an apparent value that includes the effect of the winding inductances and should not be used.

In Fig. 10, the measured winding impedances versus frequency for three different cases are shown, namely, *Case (1)*, a single phase of the motor windings; *Case (2)*, the same single phase with one end shorted to the motor frame; and *Case (3)*, one end of the same phase and frame while the other end

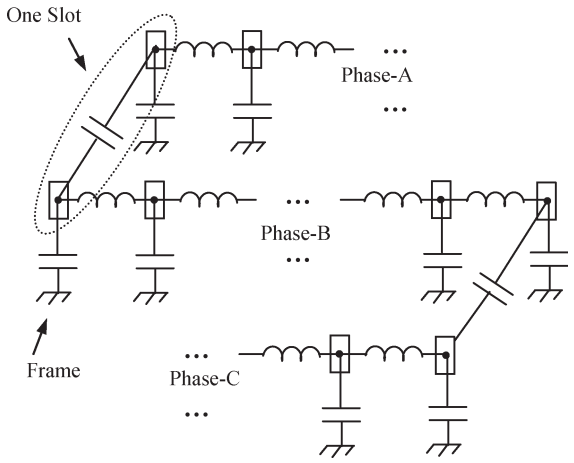

Fig. 11. Winding-to-frame and phase-to-phase stray capacitors.

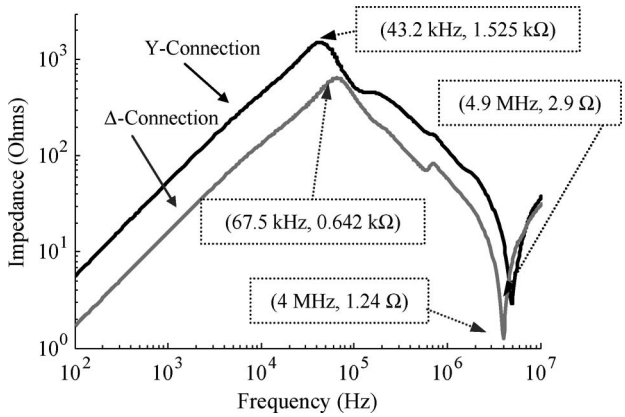

Fig. 12. Measured DM impedances of Y- and Δ-connections of the 100-hp motor versus frequency.

was completely isolated from the frame. As can be seen, the measured impedances of *Cases (2)* and *(3)* are the same at high frequencies, while the measured impedance of *Case (1)* is twice the other two cases around 1 MHz.

With reference to Fig. 11, let us assume that the impedance of phase B is measured according to *Case (2)* when one end is shorted to the frame. This means that only the slot-to-frame capacitor of one end of phase B is involved in this measurement. Whereas for *Case (1)*, two end slots have contribution to the impedance values, and the rest are electrically isolated because of the high impedance of the winding at high frequencies.

There is a fundamental difference between the sources of the effective stray capacitors in inductors and ac motors. In an inductor, particularly with a relatively thick bobbin, the turn-to-turn parasitic capacitors will bypass the winding leakage and magnetizing inductances at high frequencies. However, in the case of ac motors, the winding coils are distributed discretely in stator core slots. Moreover, these windings are very close to the surface of slots. Accordingly, the stray winding-to-frame capacitance is much bigger than the coil-to-coil stray capacitance. In other words, the winding-to-frame parasitic capacitance plays the key role, not the interturn parasitic capacitance. That means that the high-frequency currents find another path through the frame to bypass the winding inductances.

The question is that *what is the effective winding-to-frame capacitance value in the universal model?* The effective capacitance value is the capacitance value measured between one motor terminal and frame at a high frequency where the corresponding impedance phase angle has its relatively minimum value, close to -90°. However, if this capacitance value needs to be calculated analytically, then the Y- and Δ-connections has to be taken into account, in addition to the slot geometry and coil design specifications [4].

In Fig. 12, the DM impedances of Y- and Δ-connections of the 100-hp motor are shown versus frequency. Based on the previous discussions, the effective winding-to-frame capacitance in a Δ-connection is twice the Y-connection at high frequencies. Also, the effective inductance ratio between Y- and Δ-connections (converted to Y-connection) is theoretically equal to 3 at low frequencies. Accordingly, the resonance frequency ratio of the Y- versus Δ-connection would be theoretically equal to $\sqrt{(2/3)} = 0.8$. This is in good agreement with the measured values shown in Fig. 12, in which this ratio is ∼0.7. The difference between the measured and expected ratio is due to the fact that, for a Δ-connection, the DM inductance at low frequencies is slightly less than the expected value. The reason is that one phase in the Δ-connection is shorted in the DM measurement. Accordingly, the effective inductance ratio for the DMs of Y- and Δ-connections will be slightly greater than 3. For example, the 100-hp motor has a ratio of $(13.78/4.15) = 3.32$ at 250 Hz, see Fig. 12.

IV. High-Frequency Elements of Universal Model of Induction Motors

In this section, a systematic approach for determining the additional parameters required in Fig. 1 to the conventional T-equivalent circuit parameters is presented using two different methodologies. A direct measurement approach to determine parameter values and calculations based on machine geometry was performed previously in [4]. This approach required adequate machine-geometry information which is not readily available. The two new methods presented only involve simple LCR CM and DM measurements of the motor under test.

A. Analytical Approach to Determine High-Frequency Model Parameters From Measured Impedance Response

These additional components are $\eta L_{\rm ls}$, a fraction of total stator $L_{\rm ls}$ attributed to first few turns of first slot, effective winding-to-frame stray capacitance $C_{\rm sf}$ of first slot, interturn winding capacitor $C_{\rm sw}$, loss equivalent resistor $R_{\rm sw}$ at the first resonance point $R_{\rm sf}$, high-frequency stator copper skin effect resistance at f_a, and frame inductance L_f and frame resistance R_f from the slot to the J-box ground reference point. It should be noted that magnetizing inductance L_m and core-loss resistance $R_{\rm core}$ are the only parameters in the universal motor model which cannot be calculated from LCR measurements. However, these two parameters can be obtained from a no-load test or from the motor manufacturer. The manufacturer's data converted into a single-phase Y-equivalent circuit for the 100-hp motor studied herein, terminated as a Δ-connection, is given in Table III.

TABLE III
PARAMETERS OF 5-, 20-, AND 100-hp INDUCTION MOTORS PER PHASE (IN A Y-EQUIVALENT) AT POWER FREQUENCY (60 Hz)

Motor Parameters	5-hp	20-hp	100-hp
Voltage	460 V, Y-	460 V, Δ-	460 V, Δ-
Number of poles	4	4	4
$R_s\,(\Omega)$	1.410	0.267	0.030
$R_r\,(\Omega)$	1.280	0.248	0.023
$L_{ls}\,(\text{mH})$	11.350	2.910	0.653
$L_{lr}\,(\text{mH})$	15.040	4.290	0.802
$L_m\,(\text{mH})$	319	77.3	20.1
$R_{core}\,(\Omega)$	2568	990	326

The effective winding-to-frame stray capacitance $C_{\rm sf}$ can be obtained from the test results shown in Fig. 9. As one can see in Fig. 9, the $C_{\rm sf}$ for both Y- and Δ-connections is equal to 21.13 nF for frequencies below 1 kHz. However, the stator-to-frame capacitance at high frequencies in the Δ-connection is twice the Y-connection, both having much lower values in comparison with their values at low frequencies. The main resonance frequency of the so-called universal model of induction motor are obtained by shorting all series resistors, opening all parallel resistors, and solving the quadratic equation $\alpha(\omega_r^2)^2 - \beta\omega_r^2 + 1 = 0$, where $\alpha = L_{\rm ls}L_{\rm lr}C_{\rm sw}C_{\rm sf}$ and $\beta = (L_{\rm ls} + L_{\rm lr})C_{\rm sf} + L_{\rm ls}C_{\rm sw}$ yields

$$f_r = \frac{1}{2\pi}\sqrt{(\beta - \sqrt{\beta^2 - 4\alpha})/2\alpha}. \tag{1}$$

It should be noted that, in (1), the effect of the magnetizing inductance is negligible, since L_m is in parallel with the rotor leakage inductance $L_{\rm lr}$ and $L_m \gg L_{\rm lr}$. Assuming that, in the proposed motor model, the rotor leakage inductance referred to stator $L_{\rm lr}$ is equal to the stator windings' leakage inductance $L_{\rm ls}$ (i.e., $L_{\rm lr} \approx L_{\rm ls}$), (1) can be simplified as

$$\omega_r^2 L_{\rm ls} = \frac{1}{C_{\rm sw}} + \frac{1}{2}\frac{1}{C_{\rm sf}} - \sqrt{\frac{1}{C_{\rm sw}^2} + \frac{1}{4}\frac{1}{C_{\rm sf}^2}}. \tag{2}$$

Solving (2) for the interturn winding capacitor $C_{\rm sw}$ yields

$$C_{\rm sw} = \frac{2\omega_r^2 L_{\rm ls}C_{\rm sf} - 1}{\omega_r^2 L_{\rm ls}\left(\omega_r^2 L_{\rm ls}C_{\rm sf} - 1\right)}. \tag{3}$$

If the stator winding terminals are connected in the form of a Δ-connection, $C_{\rm sw}$ in a Y-equivalent circuit is obtained from the following:

$$C_{\rm sw} = \frac{2(2\omega_r)^2 L_{\rm ls}C_{\rm sf} - 1}{(2\omega_r)^2 L_{\rm ls}\left((2\omega_r)^2 L_{\rm ls}C_{\rm sf} - 1\right)}. \tag{4}$$

Knowing the effective winding-to-frame stray capacitance $C_{\rm sf}$ from LCR measurements as explained in the previous section, the interturn winding capacitor $C_{\rm sw}$ can be calculated from (3) and (4) for Y- and Δ-connections, respectively. It should be noted that the motor frequency response is mainly affected by $C_{\rm sw}$ at midfrequencies. Accordingly, in order to estimate the $C_{\rm sw}$ value at midfrequencies, $C_{\rm sw}$ is calculated for both $C_{\rm sf}$ values at low as well as high frequencies, and then, the average value is chosen as an effective value for $C_{\rm sw}$. The stator high-frequency skin effect resistance $R_{\rm sf}$ and inductance $\eta L_{\rm ls}$ are obtained from knowing antiresonance frequency f_a and the DM impedance value at the so-called antiresonance point from (5)

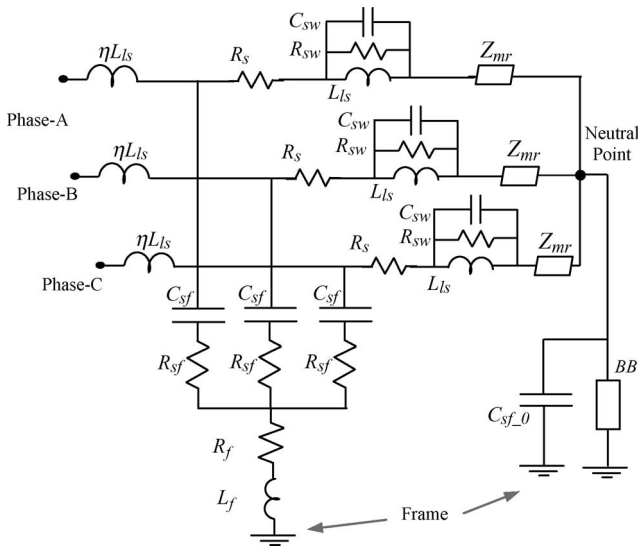

Fig. 13. Equivalent Y-connection for both actual Y- and Δ-connections of the stator windings of three-phase induction motors.

$$R_{\rm sf} = (2/3)|Z|_{\text{anti-r}} \tag{5}$$

$$\eta L_{\rm ls} = \frac{1}{C_{\rm sf}(2\pi f_a)^2}. \tag{6}$$

The value of $R_{\rm sw}$ can be estimated from the DM impedance value $|Z|_{\max}$ at the first resonance point as follows:

$$R_{\rm sw} = (2/3)|Z|_{\max} - |R_{\rm core}\|(j2\pi f_r L_{\rm lr})|\,. \tag{7}$$

The three-phase universal motor model is shown in Fig. 13 for a steady state condition or constant speed. The $Z_{\rm mr}$ parameter block corresponds to the low-frequency T-equivalent parameters in the dotted box of Fig. 1. The model block *BB* at the neutral point to ground corresponds to the previous bearing model of [4].

In order to include the total winding-to-frame stray capacitance value at low frequencies, the $C_{\text{sf-0}}$ must be added between the neutral point and frame. This capacitance is calculated as follows:

$$C_{\text{sf-0}} = \big(C_{\text{sf(LF, one-lead-to-frame)}} - 3C_{\text{sf(HF, one-lead-to-frame)}}\big)\,. \tag{8}$$

The following steps are needed to calculate the high-frequency parameters in the universal induction motor model as well as the stator and rotor leakage inductances, using measurements obtained from an LCR meter.

1) Obtain the frequency and the corresponding impedance magnitude at which the impedance phase angle has its maximum value, see Fig. 12.
2) Obtain the frequency and impedance magnitude $|Z|_{\max}$ at the first resonance point f_r, see Fig. 12.

TABLE IV
INDUCTION MOTOR MODEL PARAMETER DETERMINATION, MEASURED DATA OF THE 100-hp MOTOR (Y-CONNECTION FOR STATOR WINDINGS)

Steps	DM Magnitude |Z| in Ω	DM Phase Angle φ in degree	Frequency in kHz
(1)	13.78	86.6	0.250
(2)	1525	-5.2	43.25
(3)	2.9	-11.6	4900
	C_{sf} in nF (one lead to frame)		
(4)	1.993	-72	740
(5)	21.13	-89	1

TABLE V
INDUCTION MOTOR MODEL PARAMETER DETERMINATION, MEASURED DATA OF THE 100-hp MOTOR (Δ-CONNECTION FOR STATOR WINDINGS)

Steps	DM Magnitude |Z| in Ω	DM Phase Angle φ in degree	Frequency in kHz
(1)	4.153	86.6	0.250
(2)	642	-8.6	67.5
(3)	1.24	6.4	4000
	C_{sf} in nF (one lead to frame)		
(4)	3.97	-69	780
(5)	21.13	-89	1

TABLE VI
PARAMETERS OF 100-hp INDUCTION MOTOR OBTAINED FROM THE MEASURED DATA PROVIDED IN TABLES IV AND V

Motor Parameters	Y - connection	Δ - connection
R_s & R_r (Ω)	0.1186	0.0412
L_{ls} & L_{lr} (mH)	2.924	0.881
ηL_{ls} (μH)	0.529	0.398
R_{sf} (Ω)	1.93	0.826
R_{sw} (Ω)	401	182
C_{sf} (nF)	1.993	3.97
C_{sw} (nF)	5.85	3.73
$C_{sf\text{-}0}$ (nF)	15.15	9.22
L_f (μH)	0.529	0.398
R_f (Ω)	1.93	0.826
The following parameters are obtained from the motor manufacturer		
L_m (mH)	60	20.1
R_{core} (Ω)	978	326

3) Obtain the frequency and impedance magnitude $|Z|_{\text{anti-r}}$ at the antiresonance point f_a, see Fig. 12.
4) Obtain the winding (one-lead) to frame capacitance at high frequencies, which is the effective high-frequency stator to frame capacitance $C_{\text{sf(HF)}}$, see Fig. 9.
5) Obtain the winding (one-lead) to frame capacitance at low frequencies, which is the so-called total stator to frame capacitance $C_{\text{sf(LF)}}$, see Fig. 9.

Using (3)–(8) and obtaining the data required in the aforementioned five steps in Tables IV and V, the 100-hp motor parameters are then calculated for both Y- and Δ-connections and given in Table VI.

In Figs. 14–17, the measured and calculated DM impedance magnitudes and phase angles of the 100-hp induction motor for both Δ- and Y-connections are demonstrated. As can be seen, the calculated values are in good agreement with the measurements, particularly at low- and high-frequency spans shown in Figs. 14 and 16. The difference between the measurement and the calculated results in the midfrequency span is mainly due to the decrease in the magnetic core (steel) permeability, which leads to a significant decrease in the magnetizing inductance

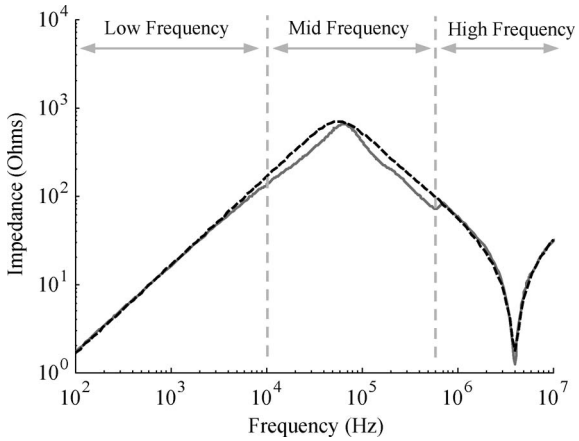

Fig. 14. (Gray) Measured versus (dashed) modeled DM impedance (magnitude) of the 100-hp motor (Δ-connection) versus frequency ($slip = 1$).

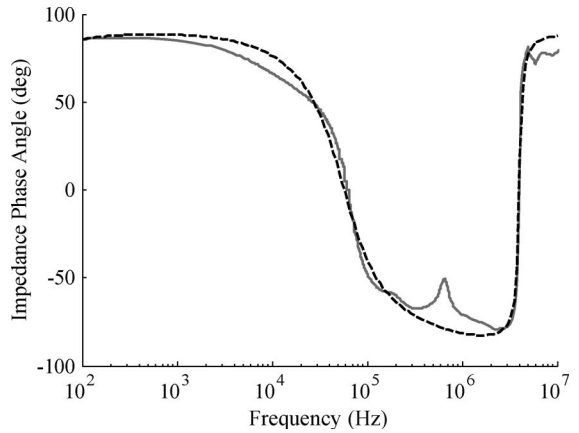

Fig. 15. (Gray) Measured versus (dashed) modeled DM impedance (phase angle) of the 100-hp motor (Δ-connection) versus frequency ($slip = 1$).

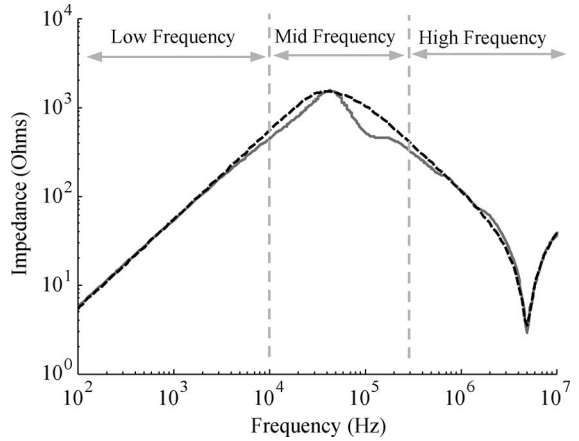

Fig. 16. (Gray) Measured versus (dashed) modeled DM impedance (magnitude) of the 100-hp motor (Y-connection) versus frequency ($slip = 1$).

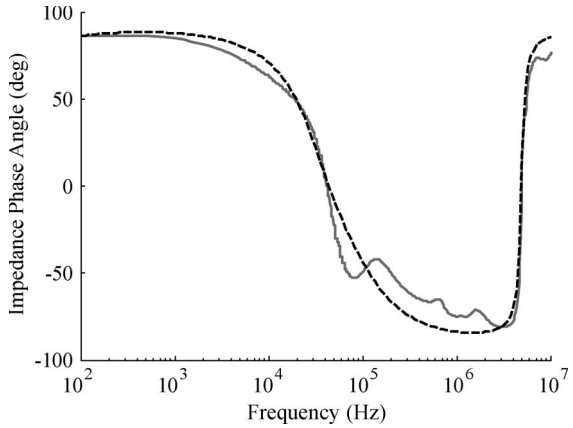

Fig. 17. (Gray) Measured versus (dashed) modeled DM impedance (phase angle) of the 100-hp motor (Y-connection) versus frequency ($slip = 1$).

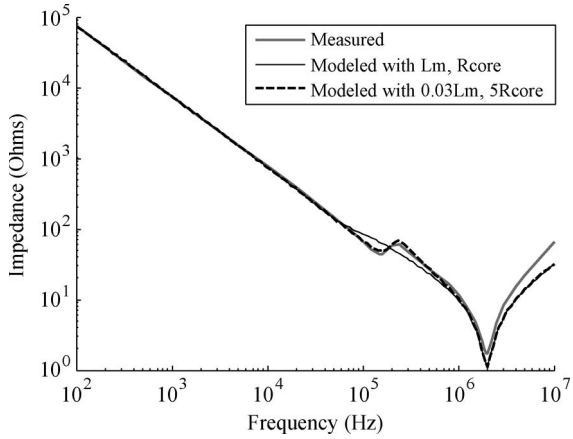

Fig. 18. (Gray) Measured versus modeled CM impedance (magnitude) of the 100-hp motor (Δ-connection) versus frequency ($slip = 1$).

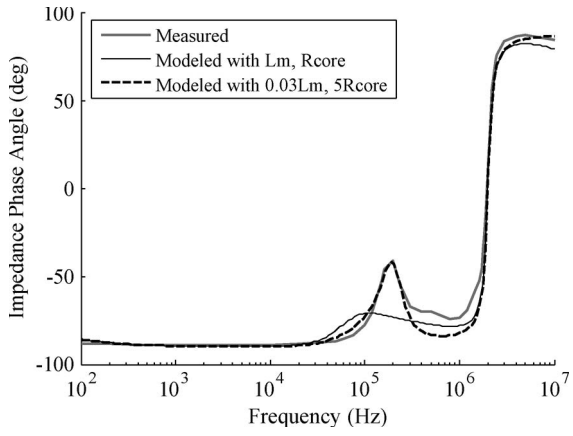

Fig. 19. (Gray) Measured versus modeled CM impedance (phase angle) of the 100-hp motor (Δ-connection) versus frequency ($slip = 1$).

L_m. However, the magnetizing inductance can be assumed constant at the low-frequency span and is not effectively a part of a circuit at the high frequencies. It should be noted that the high-frequency currents leak to the ground mainly through $\eta L_{\rm ls}$, $C_{\rm sf}$, $R_{\rm sf}$, R_f, and L_f. Accordingly, the magnetizing inductance has an insignificant impact on the effective motor impedance at high frequencies, see Fig. 13.

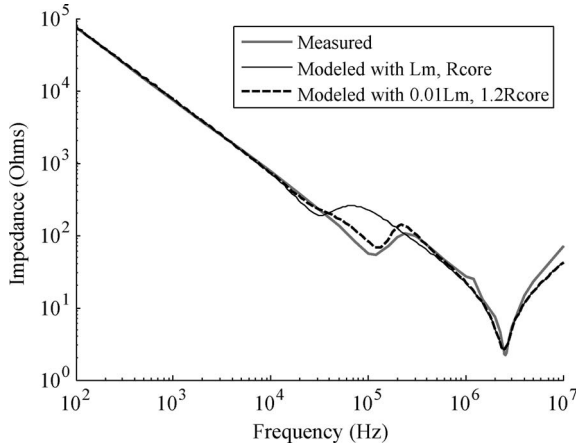

Fig. 20. (Gray) Measured versus modeled CM impedance (magnitude) of the 100-hp motor (Y-connection) versus frequency ($slip = 1$).

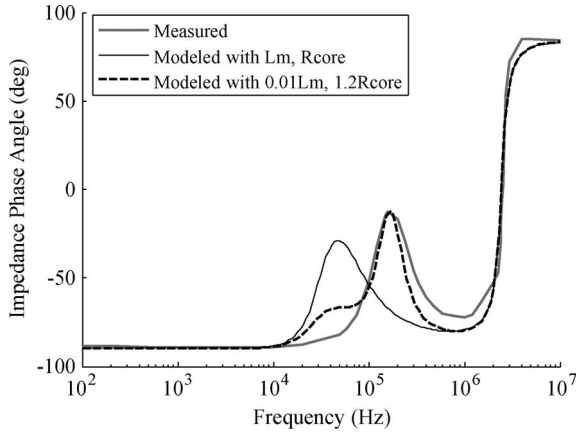

Fig. 21. (Gray) Measured versus modeled CM impedance (phase angle) of the 100-hp motor (Y-connection) versus frequency ($slip = 1$).

In Figs. 18–21, the measured and calculated CM impedance magnitudes and phase angles of a 100-hp induction motor for both Δ- and Y-connections are demonstrated. Again, the calculated values are in good agreement with the measurements particularly at low- and high-frequency domains. In the CM impedance measurements shown in Figs. 18–20, the decrease in the permeability can be observed where the motor capacitive impedance increases rapidly in the frequency range of 10–30 kHz. This phenomenon is due to the very low magnetizing inductance of the motor in CM due to magnetic coupling between the phases. To confirm this, the CM impedance response of the model are shown for a CM magnetizing inductance equal to 1% of the corresponding DM magnetizing inductance, for Δ- and Y-connections, in Figs. 18–21. As can be seen, this shows a very close match between the measured data and model response even in the midfrequency range.

B. Parameter Identification Approach to Obtain High-Frequency Model Parameters

An alternative method to obtain the high-frequency model parameters is to use a parameter identification procedure using the known circuit topology of Fig. 13 and the measured DM and CM impedances. The high-frequency model parameters of

TABLE VII
PARAMETERS OF 100-hp INDUCTION MOTOR OBTAINED FROM AN LSE

Motor Parameters	Y - connection	Δ - connection
ηL_{ls} (μH)	0.46	0.42
R_{sf} (Ω)	2.49	0.73
R_{sw} (Ω)	482	137
C_{sf} (nF)	2.3	3.8
C_{sw} (nF)	7.2	8.6
$C_{sf\text{-}0}$ (nF)	16.3	9.6
L_f (μH)	0.44	0.46
R_f (Ω)	1.63	1.57
L_m (mH) *Only for CM*	(0.00855)(60)	(0.032)(20.1)
R_{core} (Ω) *Only for CM*	(1)(978)	(2.92)(326)

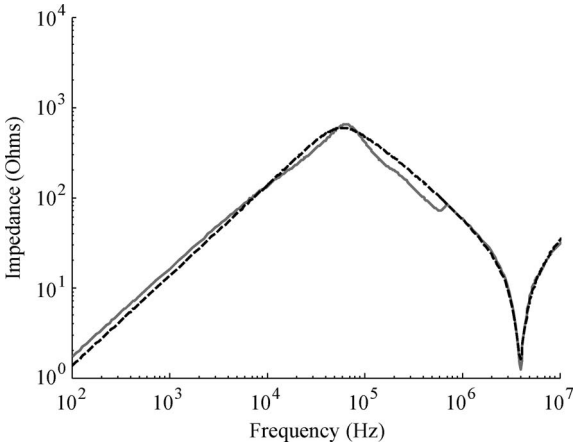

Fig. 22. (Gray) Measured versus (dashed) modeled DM impedance (magnitude) of the 100-hp motor (Δ-connection) versus frequency ($slip = 1$)—using LSE-based parameter identification.

Fig. 13, namely, $\eta L_{\rm ls}$, $R_{\rm sw}$, $C_{\rm sw}$, $C_{\rm sf}$, $C_{\rm sf\text{-}0}$, $R_{\rm sf}$, R_f, and L_f, can be determined using a least square error (LSE) approach to best fit *both* the model DM and CM impedances to measured data. It must be noted that the magnetizing inductance and core-loss resistance in CM are different from their corresponding values for DM.

The high-frequency parameters determined using LSE-based parameter identification are shown in Table VII. The parameters obtained using this approach closely matches the Table VI values determined by analytical equations and based on the resonant points in the measured impedance data. This also shows that the circuit model derived for the motor accurately represents the physical characteristics over a wide frequency range.

The measured DM and CM impedances for the Δ-connected 100-hp motor and the corresponding model values with parameters estimated using the two different approaches are shown in Figs. 22–25. It is clear that the model accurately represents the characteristics of the motor up to 10 MHz.

V. CONCLUSION

The following conclusions can be inferred from this paper.

1) A simple electromagnetic inductor was shown to have a low- to high-frequency response and model similar to a motor stator winding and was used as a basis for analyzing and modeling the proposed universal model of an induction motor.
2) The proposed universal model of an induction motor consists of adding several new parameter elements to

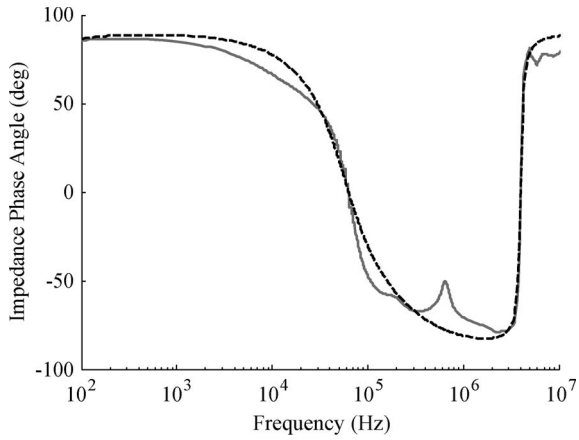

Fig. 23. (Gray) Measured versus (dashed) modeled DM impedance (phase angle) of the 100-hp motor (Δ-connection) versus frequency ($slip = 1$)—using LSE-based parameter identification.

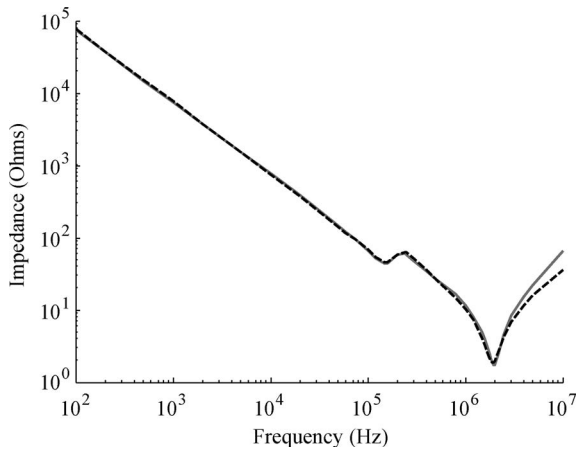

Fig. 24. (Gray) Measured versus (dashed) modeled CM impedance (magnitude) of the 100-hp motor (Δ-connection) versus frequency ($slip = 1$)—using LSE-based parameter identification.

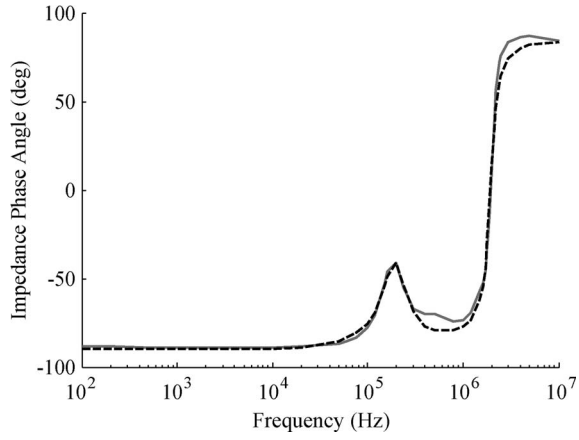

Fig. 25. (Gray) Measured versus (dashed) modeled CM impedance (phase angle) of the 100-hp motor (Δ-connection) versus frequency ($slip = 1$)—using LSE-based parameter identification.

the IEEE Standard 112 equivalent circuit low-frequency model.

3) An analysis of motor high-frequency behavior with regard to the impact of magnetic core selection, parasitic interturn and winding-to-frame capacitors, and skin effects of windings was investigated in detail for the proposed added parameters in the universal model of an induction motor. Discussion on how the new added parameters may change for Δ- and Y-stator connection windings was also provided.
4) Two new systematic procedures for determining the added model parameter elements were demonstrated.
   a) Analytical equations and resonance points in a measured CM/DM impedance versus frequency test are used, as well as only $R_{\rm core}$ and L_m from the T-equivalent circuit.
   b) The LSE-based parameter estimation approach fits the measured CM/DM impedance response to the proposed model using all known T-equivalent circuit parameters.
5) The experimental results presented show that the analytical and parameter estimation approaches result in a universal model whose impedance response at low to high frequencies up to 10 MHz closely matches the measured values, for both DM and CM. This verifies that the motor model order and element connection format assumption are correct.
6) This model can be used for a complete three-phase system simulation of the reflected-wave phenomenon, CM currents and EMI analysis, and bearing-current issues in ac motor-drive systems, including the effects of load level.

REFERENCES

[1] E. Zhong, A. Lipo, and S. Rossiter, "Transient modeling and analysis of motor terminal voltage on PWM inverter-fed AC motor drives," in *Conf. Rec. 33rd IEEE IAS Annu. Meeting*, Oct. 1998, pp. 773–780.

[2] A. F. Moreira, T. A. Lipo, G. Venkataramanan, and S. Bernet, "High-frequency modeling for cable and induction motor overvoltage studies in long cable drives," *IEEE Trans. Ind. Appl.*, vol. 38, no. 5, pp. 1297–1306, Sep./Oct. 2002.

[3] G. Suresh, A. Toliyat, A. Rendusara, and N. Enjeti, "Predicting the transient effects of PWM voltage waveform on the stator windings of random wound induction motors," *IEEE Trans. Power Electron.*, vol. 14, no. 1, pp. 23–30, Jan. 1999.

[4] B. Mirafzal, G. Skibinski, R. Tallam, D. Schlegel, and R. Lukaszewski, "Universal induction motor model with low-to-high frequency response characteristics," *IEEE Trans. Ind. Appl.*, vol. 43, no. 5, pp. 1233–1246, Sep./Oct. 2007.

[5] A. Boglietti and E. Carpaneto, "Induction motor high frequency model," in *Conf. Rec. 34th IEEE IAS Annu. Meeting*, Phoenix, AZ, Oct. 1999, pp. 1551–1558.

[6] A. Boglietti, A. Cavagnino, and M. Lazzari, "Experimental high-frequency parameter identification of AC electrical motors," *IEEE Trans. Ind. Appl.*, vol. 43, no. 1, pp. 23–29, Jan./Feb. 2007.

[7] M. Schinkel, S. Weber, S. Guttowski, W. John, and H. Reichl, "Efficient HF modeling and model parameterization of induction machines for time and frequency domain simulations," in *Proc. IEEE Appl. Power Electron. Conf.*, Mar. 2006, pp. 1181–1186.

[8] R. Kerkman, D. Leggate, and G. Skibinski, "Interaction of drive modulation and cable parameters on ac motor transients," in *Conf. Rec. 31st IEEE IAS Annu. Meeting*, Oct. 1996, pp. 143–152.

[9] L. Ran, S. Gokani, J. Clare, K. J. Bradley, and C. Christopoulos, "Conducted electromagnetic emissions in induction motor drive systems. I. Time domain analysis and identification of dominant modes," *IEEE Trans. Power Electron.*, vol. 13, no. 4, pp. 757–767, Jul. 1998.

[10] A. deBroe, A. Julian, and T. Lipo, "Neutral-to-ground voltage minimization in a PWM rectifier/inverter configuration," WEMPEC, Madison, WI, pp. 12–96, Res. Rep.

[11] *IEEE Standard 112 Test Methods For AC Induction Motors*.

[12] A. E. Fitzgerald, C. Kingsley, and S. D. Umans, *Electric Machinery*, 6th ed. New York: McGraw-Hill, 2003.

Behrooz Mirafzal (S'01–M'05–SM'07) received the B.Sc. degree from Isfahan University of Technology, Isfahan, Iran, in 1994, the M.Sc. degree (with first-class honors) from the University of Mazandaran, Mazandaran, Iran, in 1997, and the Ph.D. degree from Marquette University, Milwaukee, WI, in 2005, all in electrical engineering.

From 1997 to 2000, he was a Research Engineer, as well as a Lecturer, with several academic institutions in Isfahan, Iran. From 2005 to 2008, he was a Senior Development/Project Engineer with Allen-Bradley Drives Division, Rockwell Automation, Mequon, WI. Since August 2008, he has been an Assistant Professor with the Department of Electrical and Computer Engineering, Florida International University, Miami. His current research interests include power electronic applications in renewable energy conversion systems and motor drives. He is the author or a coauthor of more than 20 conference and journal papers. He is the holder of one U.S. patent, with two others pending.

Gary L. Skibinski received the B.S.E.E. and M.S.E.E. degrees from the University of Wisconsin, Milwaukee, and the Ph.D. degree from the University of Wisconsin, Madison, in 1976, 1980, and 1992, respectively.

From 1976 to 1980, he was an Electrical Engineer working on naval nuclear power with Eaton Corporation, Cleveland, OH. From 1981 to 1985, he was a Senior Project Engineer with Allen-Bradley Company, Inc., where his work concerned servo controllers. During the Ph.D. program, he was a Consultant for uninterruptible power system and switch-mode power supply products with R.T.E. Corporation. He is currently an Engineering Consultant with Allen-Bradley Drives Division, Rockwell Automation, Mequon, WI. His current interests include power semiconductors, power electronic applications, and high-frequency high-power converter circuits for ac drives. He has published over 80 articles in professional journals and conferences with 18 winning prize awards. He holds 19 U.S. patents.

Rangarajan M. Tallam (S'97–M'01–SM'07) received the B.Tech. degree in electrical engineering from the Indian Institute of Technology, Madras, India, and the M.S.E.E. and Ph.D. degrees in electrical engineering from the Georgia Institute of Technology, Atlanta, in 1997, 1999, and 2001, respectively.

From 2001 to 2005, he was a Senior Research Engineer with the Advanced Technology Division, Rockwell Automation, Milwaukee, WI, where he conducted research on active rectifiers and multilevel converters. He is currently a Senior Project Engineer with Allen-Bradley Drives Division, Rockwell Automation, Mequon, WI. His research interests are in switching power converter technology, motor control, and alternating current drive systems. He holds four U.S. patents.